Flexible PVDF-TrFE Nanocomposites with Ag-decorated BCZT

Heterostructures for Piezoelectric Nanogenerator Applications

Mingyang Yan[†], Shengwen Liu[†], Yuan Liu[†], Zhida Xiao[†], Xi Yuan^{‡*}, Di Zhai[†], Kechao Zhou[†], Qingping Wang[§], Dou Zhang[†], Chris Bowen[§] and Yan Zhang^{†*}

† State Key Laboratory of Powder Metallurgy, Central South University, Changsha, Hunan 410083, China.

‡ College of Chemistry and Chemical Engineering, Central South University, Changsha, Hunan 410083, China.

§ Department of Mechanical Engineering, University of Bath, United Kingdom, Bath,

BA2 7AY, UK

Corresponding Authors

* E-mail: yanzhangcsu@csu.edu.cn (Yan Zhang).

Abstract

Flexible piezoelectric nanogenerators are playing an important role in delivering power to next generation wearable electronic devices due to their high-power density and potential to create self-powered sensors for the Internet of Things. Among the range of available piezoelectric materials, poly(vinylidene fluoride-trifluoroethylene) (PVDF-TrFE) based piezoelectric composites exhibit significant potential for flexible piezoelectric nanogenerator applications. However, the high electric fields that are

^{*} E-mail: xiyuan@csu.edu.cn (Xi Yuan).

required for poling cannot be readily applied to polymer composites containing piezoelectric fillers due to the high permittivity contrast between the filler and matrix, which reduces the dielectric strength. In this paper, novel Ag-decorated BCZT heterostructures were synthesized via a photo-reduction method, which were introduced at a low level (3 wt.%) into the matrix of poly-[(vinylidene fluoride)-co-trifluoroethylene] (PVDF-TrFE) to fabricate piezoelectric composite films. The effect of Ag nanoparticle loading content on the dielectric, ferroelectric and piezoelectric properties was investigated in detail, where a maximum piezoelectric energy harvesting figure of merit of 5.68×10⁻¹² m²/N was obtained in a 0.04Ag-BCZT NWs/PVDF-TrFE composite film; where 0.04 represents the concentration of the AgNO₃ solution. Modelling showed that an optimum performance was achieved by tailoring the fraction and distribution of the conductive silver nanoparticles to achieve a careful balance between generating electric field concentrations to increase the level of polarization, while not degrading the dielectric strength. This work therefore provides a strategy for the design and manufacture of highly polarized piezoelectric composite films for piezoelectric nanogenerator applications.

Key words: Ag nanoparticles, BCZT nanowires, heterostructures, piezoelectric composite, energy harvesting

1. Introduction

The increasing energy crisis and growing need for sensor systems for the Internet

of Things have become a significant challenge in our society.¹⁻³ In our living environment, there are many ambient forms of energy sources, which includes light, heat, wind and mechanical vibrations. Piezoelectric nanogenerators, which are able to convert mechanical energy sources into electricity, have attracted significant interest in recent years due to their high-power density, mechanical stability, low density and low cost.⁴⁻⁷ As a result, piezoelectric nanogenerators are promising candidates for powering wearable sensors and electronic devices.

Piezoelectric materials are playing an important role in the development of piezoelectric nanogenerators, and the selection of the appropriate piezoelectric material can greatly influence the performance, and ultimately their applications. Compared to piezoelectric ceramics and polymers, piezoelectric composites, which aim to combine the high piezoelectric coefficient of piezoelectric ceramics and the high flexibility of polymers, exhibit significant potential for piezoelectric nanogenerator applications. Among the range of piezoelectric composites that have been studied, poly(vinylidene fluoride) (PVDF) based composites have attracted much attention. Poly-[(vinylidene fluoride)-co-trifluoroethylene] (PVDF-TrFE), as a copolymer of PVDF, has been explored as the matrix of piezoelectric composites due to its relatively high piezoelectric coefficient and high degree of mechanical flexibility. 12, 13

In recent decades, significant effort has been paid to the investigation of PVDF-TrFE composites based piezoelectric nanogenerators. A variety of piezoelectric ceramic fillers have been selected to fabricate piezoelectric composites; these include

lead zirconate titanate (PZT)¹⁴, lead magnesium niobate-lead titanate (PMN-PT)¹⁵, potassium sodium niobate (KNN)¹⁶, barium calcium zirconate titanate (BCZT)¹⁷. Wu et al. prepared PVDF-TrFE-based piezoelectric composite films containing PZT powder and graphene nanosheets. A maximum power density of 1.4 µW/cm² was obtained when the loading content of PZT powders reached 15 wt%. ¹⁸ A piezoelectric organic-inorganic hybrid nanocomposite film was fabricated by mixing BaTiO₃ nanoparticles within a PVDF-TrFE matrix, and the maximum output power density was measured to be 18.4 µW/cm², which is 4.8 times higher than that of pure PVDF-TrFE film.¹⁹ In addition to the type of piezoelectric ceramic fillers, the micro-morphology of the filler also plays an important role on the performance of piezoelectric composite nanogenerators.²⁰ In general, piezoelectric fillers can be classified into four types, including zero-dimensional (0D) piezoelectric nanoparticles²¹, one-dimensional (1D) piezoelectric nanowires or fibers²², two-dimensional (2D) piezoelectric nanosheets²³ and three-dimensional (3D) piezoelectric nanoflowers or bulk materials²⁴. Compared with 0D piezoelectric nanoparticles, 1D and 2D piezoelectric fillers exhibit potential piezoelectric nanogenerators due to their increased connectivity in a particular dimension. The dielectric constant and polarization strength of nanocomposite films can be enhanced as a result of the large dipole moment of 1D and 2D piezoelectric fillers.^{25, 26} For example, for PZT- and BaTiO₃-based materials the piezoelectric activity in nanowire form is higher than that of other morphologies. 27, 28 In addition, it was demonstrated that 1D and 2D piezoelectric fillers have a lower surface area than 0D fillers, which

helps reduce the surface energy and inhibits agglomeration in nanocomposite films.²⁹ Moreover, 1D and 2D piezoelectric materials can be oriented in a polymer matrix via a tape casting process to fabricate piezoelectric nanogenerators with excellent performance due to their highly preferred orientation.³⁰ Therefore, the use of one-dimensional piezoelectric fillers is a topic of research interest.

The addition of electrically conductive materials is also considered to be an effective approach to enhance the output performance of piezoelectric nanogenerators. Conductive materials that have been examined to date include silver nanoparticles and nanowires, carbon nanotubes, graphene, and graphene quantum dots. 31, 32 For example, Shi et al. fabricated a flexible piezoelectric nanogenerator via an electrospinning method, which was composed of 0.15 wt% graphene nanosheets and 15 wt% BaTiO₃ nanoparticles. The open-circuit voltage and the maximum output power of the piezoelectric nanogenerator was 11 V and 4.1 μW respectively. ³³ Subsequently, Zhou et al. synthesized porous Ag nanowire/PVDF-TrFE piezoelectric composites via a simple etching template method, and a high output power density of 7.1 µW/cm² was achieved using this piezoelectric nanogenerator.³⁴ Despite the enhancement of piezoelectric output and properties, an inhomogeneous distribution of conductive filler material and poor contact between the piezoelectric and conductive filler can have a negative effect on the electric field distribution within the composite during the poling process.³⁵ This includes the formation of electric field concentrations that can lead to dielectric breakdown or low electric field regions that exhibit low levels of polarization during poling. The mechanical property mismatch, such as stiffness,

between the piezoelectric ceramic fillers, polymer matrix and conductive materials is also a challenge for improving the output performance of piezoelectric nanogenerators. Recently, a novel strategy was proposed by depositing a layer of conductive nanoparticles on the surface of piezoelectric ceramic fillers to improve performance. For example, a carbon layer was deposited on BaTiO₃ (BT) nanoparticles to form a core-shell structure; the nanoparticles were then introduced into a PVDF-TrFE matrix to fabricate a piezoelectric nanogenerator. A maximum output power of 2.4 µW/cm² was achieved with a 15 wt % BT@C/P(VDF-TrFE) piezoelectric nanogenerator.³⁶ Shuai et al. synthesized strawberry-structured Ag-BT nanoparticles and introduced them into a PVDF scaffold by a selective laser sintering method. The piezoelectric voltage of PVDF/4Ag-BT scaffold was 1.5 times higher than that of pure PVDF/BT scaffold.³⁷ These results demonstrate that the deposition of a conductive layer on a piezoelectric filler can enhance the performance of piezoelectric nanogenerators. Nevertheless, a number of challenges remain to be solved; where a high piezoelectric filler loading content is currently needed to achieve a high piezoelectric coefficient, ranging from 20 to 50 wt%. The addition of such a high content of piezoelectric ceramic can lead to agglomeration of the filler with the polymer matrix, which can negatively affect the internal electric field distribution and mechanical flexibility of the composite film.³⁸

BCZT is lead-free and environmentally-friendly ferroelectric with low toxicity to the environment and humans, where high piezoelectric coefficients have been reported $(d_{33}\approx755 \text{ pC/N})$. This ferroelectric material therefore provides a route for

the development of high performance and lead-free piezoelectric nanogenerators. Experiments have shown that the material can be used to fabricate piezoelectric composites when embedded in both PVDF and poly(methyl methacrylate) (PMMA)-based matrices, which have also included conductive Ag fillers. It was demonstrated that the polarization, conductivity and current density of BCZT+Ag/PVDF and BCZT+Ag/40%PMMA/PVDF was enhanced compared to piezoelectric composites without conductive Ag fillers. In addition, BCZT ceramic particles have been embedded in a PVDF-TrFE polymer to form a composite, which demonstrated that the polarization and mechanical strength are enhanced at a BCZT volume fraction of 0.2. However, the use of high volume fractions of BCZT makes it difficult to disperse in the polymer matrix, which leads to agglomeration and the formation of defects; clearly there is a benefit in using small fractions of piezoelectric filler to tailor the properties.

In this paper, a new approach is developed to create piezoelectric composites, where silver nanoparticles are decorated on Ba_{0.85}Ca_{0.15}Ti_{0.9}Zr_{0.1}O₃ nanowires (BCZT NWs) via a photo-reduction method and a low-level of 3 wt% piezoelectric ceramic fillers were introduced in a PVDF-TrFE matrix to fabricate flexible piezoelectric nanogenerator. The effect of Ag nanoparticle loading content on the dielectric, ferroelectric, piezoelectric properties was investigated in detail and the impact of composite structure on the electric field distribution within the composite microstructure was modelled. A maximum piezoelectric energy harvesting figures of merit was obtained by achieving an optimum balance between Ag content,

conductivity, and dielectric strength. The energy harvesting performance figure of merit was increased by 49% for the Ag-loaded composite, where this work provides a new strategy to enhance the output performance of piezoelectric nanogenerators.

2. Experimental Section

2.1 Synthesis of $Ba_{0.85}Ca_{0.15}Ti_{0.9}Zr_{0.1}O_3$ (BCZT) nanowires (NWs)

The BCZT nanowires (NWs) were synthesized via a combination of sol-gel and electrospinning method. Firstly, analytical grades of barium acetate (99.99%, calcium acetate monohydrate (99%, Macklin), Macklin), and zirconium acetylacetonate (98%, Macklin), were weighed according to the required molar ratio and dissolved in the mixed solvent of acetic acid (98%, Sinopharm) and ethylene glycol monomethyl ether (98%, Sinopharm). Then, acetylacetone and tetrabutyl titanate (98.0%, Sinopharm) was added to the solution and stirred for 6 h at 40 °C to form a homogeneous sol. The electrospinning precursor solution was prepared by adding polyvinylpyrrolidone (PVP, M_w=1300000, Macklin, Shanghai, China) to the sol and stirred for 6 h, and the mass ratio of PVP and BCZT sol was 1.5:10. The electrospinning parameters were a voltage of 10 kV, an injection rate of 1.2 ml/h, and a pinhead-to-collector distance of 15 cm. Finally, the as-spun nanowires were calcined at 400 °C for 1 h and sintered at 800 °C for 2 h to obtain high aspect ratio BCZT NWs.

2.2 Preparation of Ag-BCZT heterostructures

The Ag-BCZT heterostructures were prepared via a facile photo-reduction method. The BCZT NWs were dispersed in ethanol solution and stirred at room

temperature for 1 h to make them uniformly dispersed in the solution. Then, different weights of silver nitrate powder were added to obtain 0.01, 0.02, 0.03, 0.04, and 0.05 M AgNO₃ solution. Subsequently, the mixture was exposed to a 300 W Xenon lamp for 45 min under a constant stirring in the dark. Finally, the powder was washed with deionized water for several times and dried in the vacuum oven at 60 °C for 12 h. The obtained samples were labeled as xAg-BCZT NWs (where x represents the concentration of AgNO₃ solution, and x = 0.01, 0.02, 0.03, 0.04, 0.05).

2.3 Fabrication of Ag-BCZT/PVDF-TrFE composites piezoelectric nanogenerator

Firstly, the Ag-BCZT NWs/PVDF-TrFE composite films were fabricated via a tape casting method. A mass of 2 g PVDF-TrFE powder was dissolved in 18 ml dimethylsulfoxide (DMSO) solvent by magnetic stirring for 6 h at 40 °C. Then, a low-level of 3 wt% xAg-BCZT nanowires was added to the PVDF-TrFE solution and sonicated for 1 h to make them dispersed uniformly in the solution. Subsequently, the suspension was coated on the glass substrate via a facile tape casting method and dried at 70 °C for 24 h in the vacuum oven to evaporate the solvent. The Ag-BCZT NWs/PVDF-TrFE composite films were then peeled from the substrate and annealed at 140 °C to eliminate closed pores and to further increase the degree of crystallinity of PVDF-TrFE.

The fabricated Ag-BCZT NWs/PVDF-TrFE composite films were cut into rectangular pieces with the dimension of $1.5 \times 2 \text{ cm}^2$. Aluminum foils were attached to the top and bottom sides of the films to form upper and lower electrodes. The composite films were polarized under a high electric field of 50 kV/mm at 60 °C

in an oil bath for 6 h. Then, silver wires were pasted on the electrodes, and polyimide (PI) films were used to package the composite film to protect them from harmful environment, and the whole structure was compressed to hinder the influence of triboelectricity between different films.

2.4 Finite element simulation analysis

COMSOL Multiphysics 5.4 (combinations of Solid Mechanics, Electrostatics, and Electrical Circuit Modules) was used to evaluate the electric field and piezoelectric potential distribution of the Ag-BCZT NWs/PVDF-TrFE composite film. The dielectric constant (ε_r) of the BCZT nanowires and PVDF-TrFE matrix were assumed to be $\varepsilon_r = 2900$ and $\varepsilon_r = 11$, respectively. Correspondingly, two two-dimensional models were created, where the dimension of the films was 72×72 µm, and the diameter of the spherical silver nanoparticles was assumed be $70 \sim 130$ nm. The diameter and the aspect ratio of the BCZT nanowires were assumed to be 300 nm and 8, respectively. An electric field of 30 kV/mm was applied to investigate the effect of Ag nanoparticles on the electric field distribution within the composite. In addition, a load of 10 N was applied to the upper surface with the lower set to ground (0V) to explore the piezoelectric potential distribution of the composite films.

2.5 Characterization and measurements

The microstructure and morphology of xAg-BCZT NWs and BCZT NWs/PVDF-TrFE composite films were observed by field emission scanning electron microscopy (FESEM, NovaNanoSEM230, USA). The microstructure of 0.04Ag-BCZT nanowires was analyzed by a high-resolution transmission microscopy

(HRTEM Titan G260-300). The crystal structure of xAg-BCZT NWs and PVDF-TrFE composite films were evaluated by X-ray diffraction (XRD) analysis with Cu Ka radiation. X-ray photoelectron spectroscopy (XPS, ThermoFisher Scientific Escalab250Xi) was used to detect the element type of Ag-BCZT NWs. The chemical structure and functional group of the Ag-BCZT NWs/PVDF-TrFE composite films were characterized by Fourier-transform infrared spectroscopy (FT-IR, VERTEX 70 V). The dielectric constant, dielectric loss and conductivity of the composite films were measured by Precision Impedance Analyzer (4294A; Agilent Technologies, Santa Clara, USA). The ferroelectric polarization-electric field (P-E) loops were characterized by a TF Analyzer 3000 (AixACCT systems, Germany). The piezoelectric charge coefficient d₃₃ was measured using a piezoelectric d₃₃ meter (ZJ-4AN, Institute of Acoustics, Academic Sinica, China). The piezoelectric output performance of the Ag-BCZT NWs/PVDF-TrFE composites was evaluated in detail. A periodic compressive stress at a specific frequency was applied through an electrodynamic shaker. The output voltage and current of the flexible piezoelectric nanogenerator were measured by a Keithley 6517B electrometer.

3. Results and discussion

Figure 1a shows the fabrication process of the flexible piezoelectric nanogenerator based on Ag-BCZT NWs/PVDF-TrFE composite films; detailed information is provided in the Experimental Section. Firstly, BCZT nanowires were synthesized by an electrospinning method, as shown in **Figure 1**a (i) and (ii). Then, silver nanoparticles were deposited on BCZT nanowires via a photo-reduction method

to obtain the Ag-BCZT heterostructures, see **Figure 1**a (iii) and (iv). Subsequently, the PVDF-TrFE powders were dissolved in dimethyl sulfoxide (DMSO), and the xAg-BCZT nanowires were dispersed in a solution to form a homogeneous suspension, as shown in **Figure 1**a (v). The prepared suspension was then tape cast onto a glass substrate, and the xAg-BCZT/PVDF-TrFE composite films were removed from the substrate after the evaporation of solvent; see **Figure 1**a (vi) and (vii). Finally, the xAg-BCZT/PVDF-TrFE composite films were polarized at an electric field of 50 kV/mm. A schematic of the flexible piezoelectric nanogenerator is presented in **Figure 1**b, where the composite film was sandwiched between two aluminum electrodes and laminated with polyimide (PI) films, and two conductive wires were connected to the electrodes to form the flexible piezoelectric nanogenerator. It can be seen from **Figure 1**c and **Figure 1**d that the Ag-BCZT NWs/PVDF-TrFE film and the flexible piezoelectric nanogenerator possessed a high degree of mechanical flexibility.

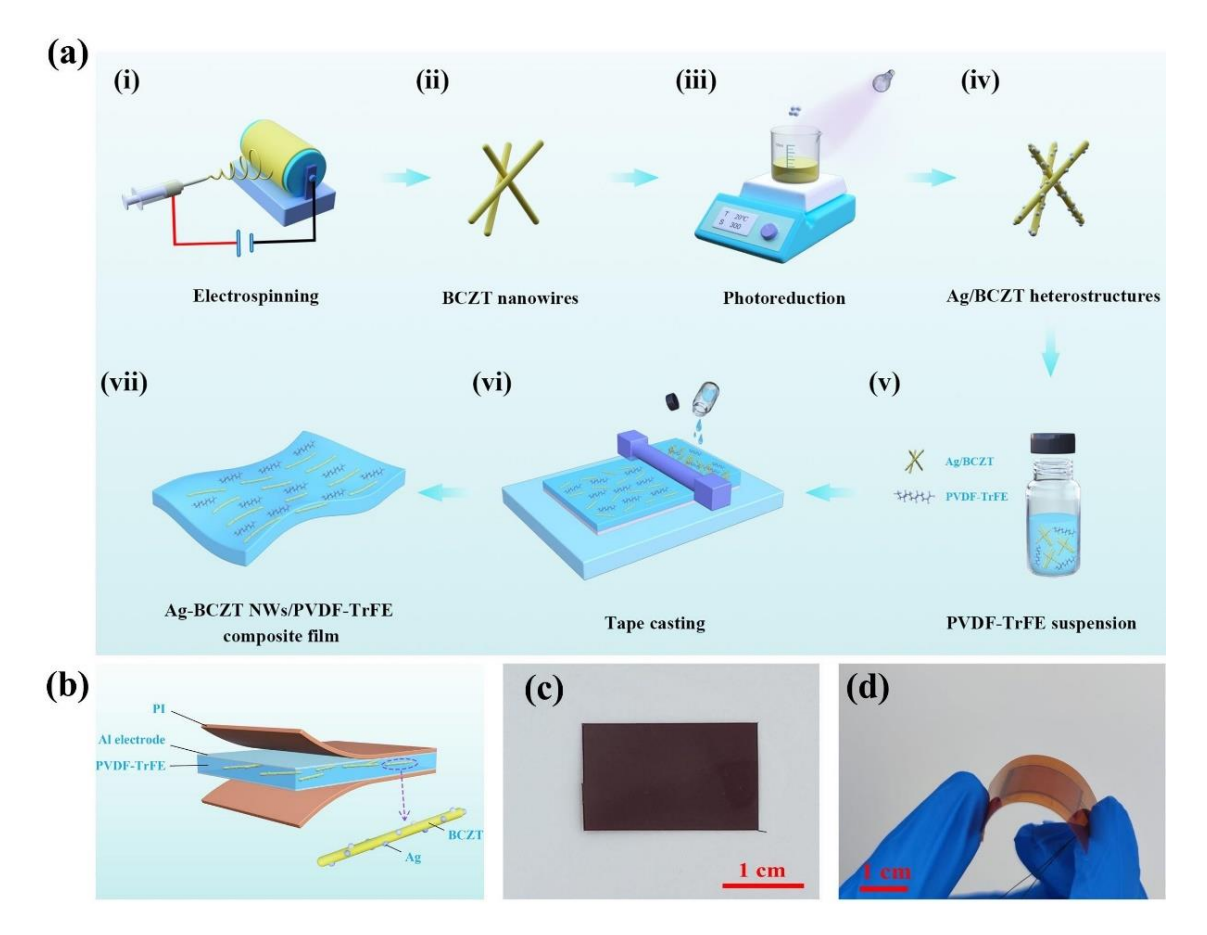


Figure 1. (a) Illustration for the fabrication process of Ag-BCZT NWs/PVDF-TrFE composite films: (i) Electrospinning of BCZT sol; (ii) BCZT nanowires; (iii) Deposition of Ag nanoparticles on BCZT nanowires; (iv) Ag/BCZT heterostructures; (v) Preparation of Ag-BCZT NWs/PVDF-TrFE suspension; (vi) Tape casting process; (vii) Ag-BCZT NWs/PVDF-TrFE composite film. (b) Schematic of the flexible piezoelectric nanogenerator. Photographs of (c) PVDF-TrFE composite film and (d) Piezoelectric nanogenerator.

SEM and TEM images of the Ag-BCZT NWs are presented in **Figure 2**, where it can be observed from **Figure 2** at that the surface of pure BCZT NWs is relatively smooth. After the photo-reduction process, spherical silver nanoparticles can be observed on the surface of BCZT NWs, as shown in **Figure 2**b-f. Moreover, the

amount of silver nanoparticles increased significantly with an increase in concentration of silver nitrate solution. In particular, for the 0.05Ag-BCZT NWs samples, some silver nanoparticles begin to interconnect with each other, and a degree of agglomeration can be observed. TEM was performed to further analyze the detailed crystalline structures of the Ag-BCZT NWs. As shown in **Figure 2**g and **2**h, silver nanoparticles can be readily observed on the surface of BCZT NWs. The crystal plane spacing is 0.291 nm, which corresponds to the (110) crystal planes of BCZT perovskite structure. The inter-planar spacing of the decorated nanoparticles is 0.237 nm, which can be assigned to the (111) crystal plane of metallic Ag. Figure 2i shows Energy Dispersive Spectroscopy (EDS) mapping analysis of the 0.04Ag-BCZT NWs. The elements of Ba, Ca, Zr, Ti, and Ag are detected by EDS, and these elements are homogeneously distributed in Ag-BCZT NWs heterostructures. These results demonstrate that silver nanoparticles were successfully deposited on BCZT NWs.

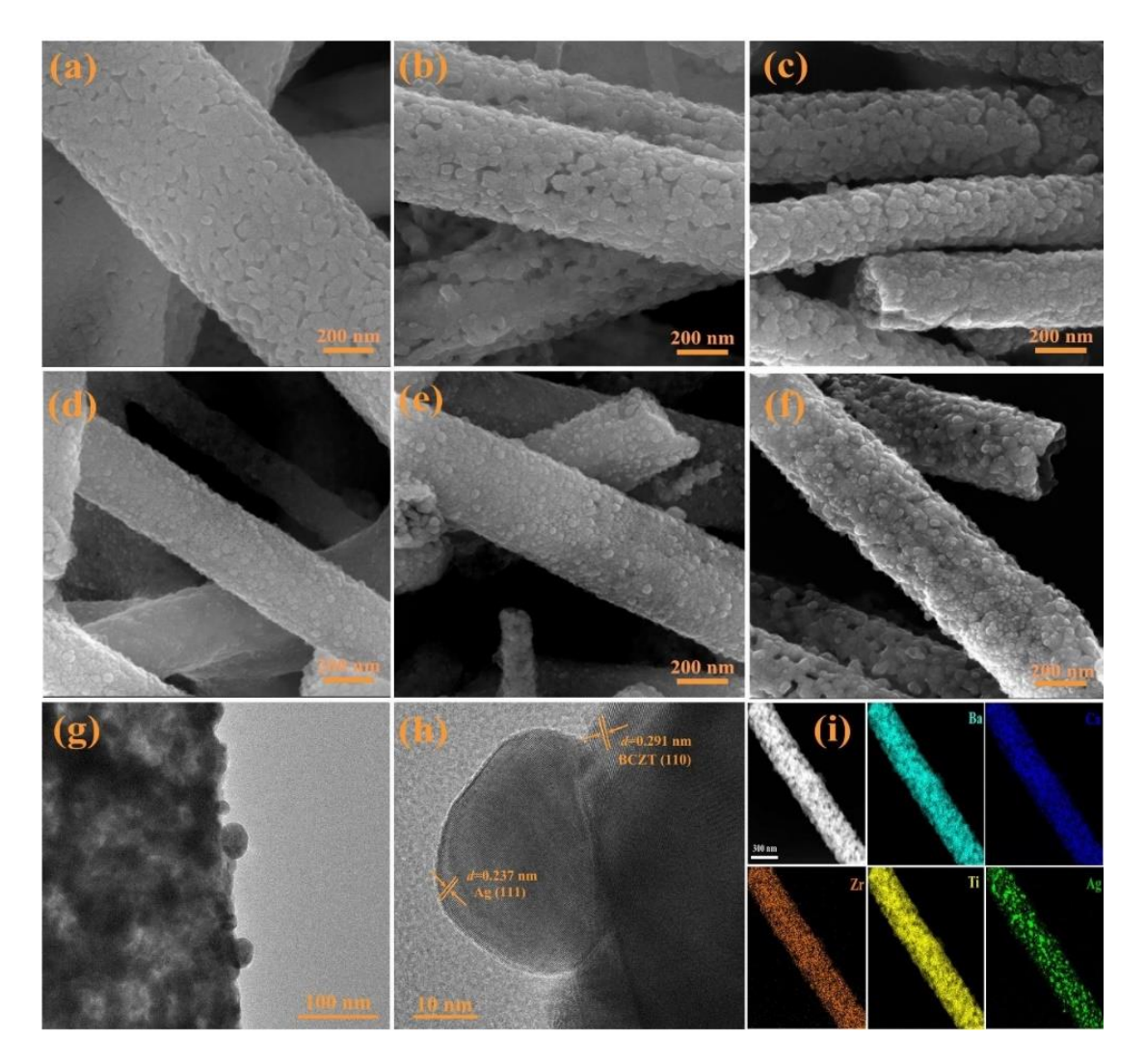


Figure 2. SEM images of the BCZT NWs with a range of Ag nanoparticle loading content. (a) Pure BCZT NWs. (b) 0.01Ag-BCZT NWs. (c) 0.02Ag-BCZT NWs. (d) 0.03Ag-BCZT NWs. (e) 0.04Ag-BCZT NWs. (f) 0.05Ag-BCZT NWs. (g-h) HRTEM images and (i) EDS mapping of the 0.04Ag-BCZT NWs.

Figure 3a and **3**b show the XRD patterns of pure BCZT NWs and xAg-BCZT NWs. It can be observed that all the diffraction peaks can be matched with the perovskite-structure of BCZT. Compared with pure BCZT NWs, characteristic diffraction peaks of metal Ag located at 38.1 and 44.3° can be observed in the samples of 0.04Ag-BCZT NWs and 0.05Ag-BCZT NWs,⁴⁴ while they are absent when the concentration of silver nitrate is lower than 0.04M. Moreover, the XRD

results are in good agreement with the inter-planar spacing in HRTEM results. The XPS spectra of pure BCZT NWs and 0.04Ag-BCZT NWs were measured to analyze the chemical bonding state of the Ag nanoparticles. As shown in **Figure 3**c, all peaks that belong to Ba 3d, Ca 2p, Zr 3d, Ti 2p, and O 1s can be observed from the scan spectra. Compared with pure BCZT NWs, peaks of Ag can be clearly observed. High resolution Ag 3d XPS peaks of 0.04Ag-BCZT NWs is shown in **Figure 3**d, where it can be seen that the peaks of Ag 3d_{3/2} and Ag 3d_{2/5} located at 374.2 and 368.1 eV, respectively, which demonstrated the existence of metallic Ag.^{16, 37} These results indicate that metallic silver nanoparticles were successfully decorated on BCZT NWs.

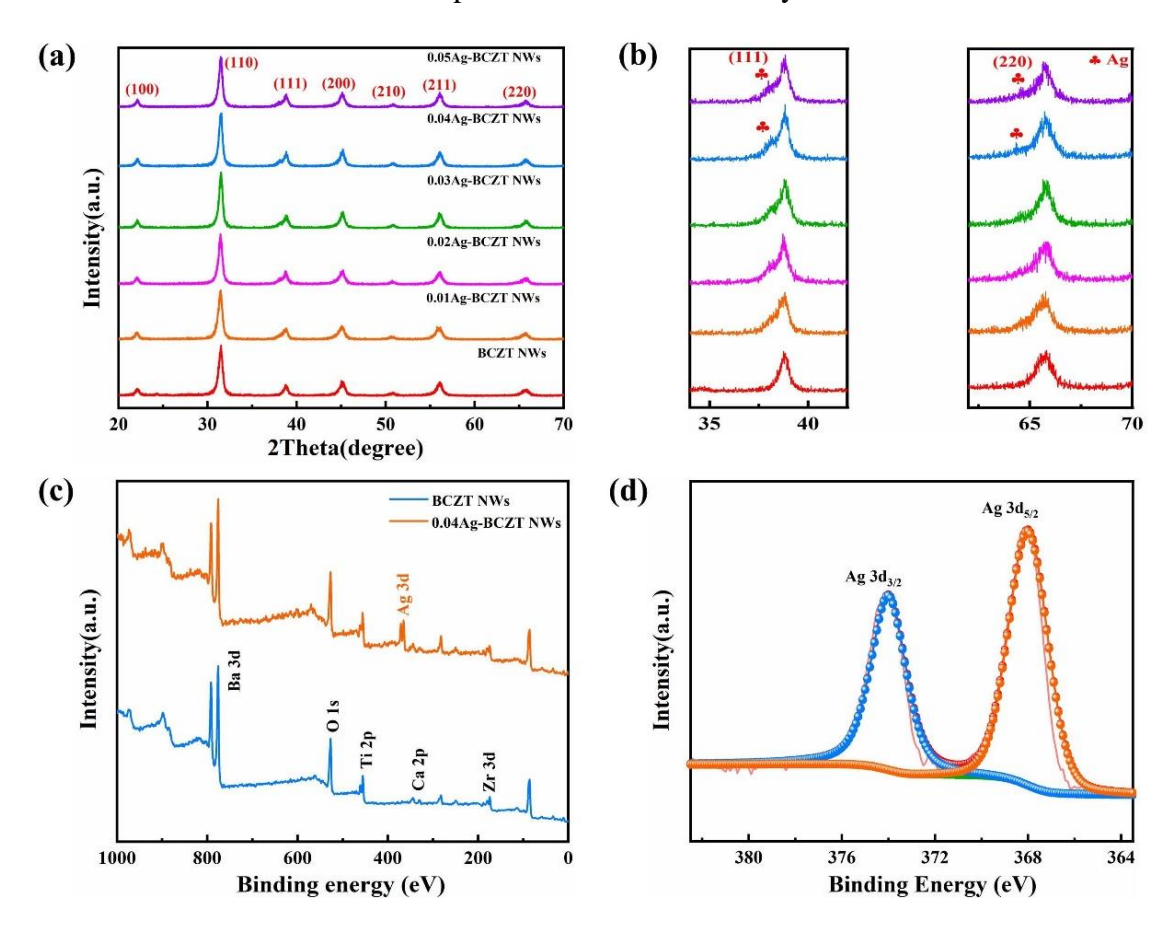


Figure 3. (a)(b) XRD patterns of the xAg-BCZT NWs. (c) XPS spectra of pure BCZT NWs and 0.04Ag-BCZT NWs. (d) High resolution XPS peaks of Ag 3d.

A facile tape casting method was applied to fabricate PVDF-TrFE composite

films containing 3wt% Ag-BCZT NWs with a range of x values (x = 0, 0.01, 0.02, 0.03, 0.04 and 0.05). The surface morphologies of the composite films are presented in **Figure 4**. It can be observed that the nanowires are uniformly distributed in the PVDF-TrFE matrix, and no agglomeration can be found. Moreover, all the composite films exhibit a dense and smooth surface, with no obvious pores and other defects, demonstrating the high quality of the prepared films. Cross-sectional SEM images of PVDF-TrFE composite films are shown in **Figure S1**, and the thickness of the composite films is approximately 30 μ m, and a relatively dense cross section can be observed, which is beneficial to enhance the piezoelectric performance of the composite films.

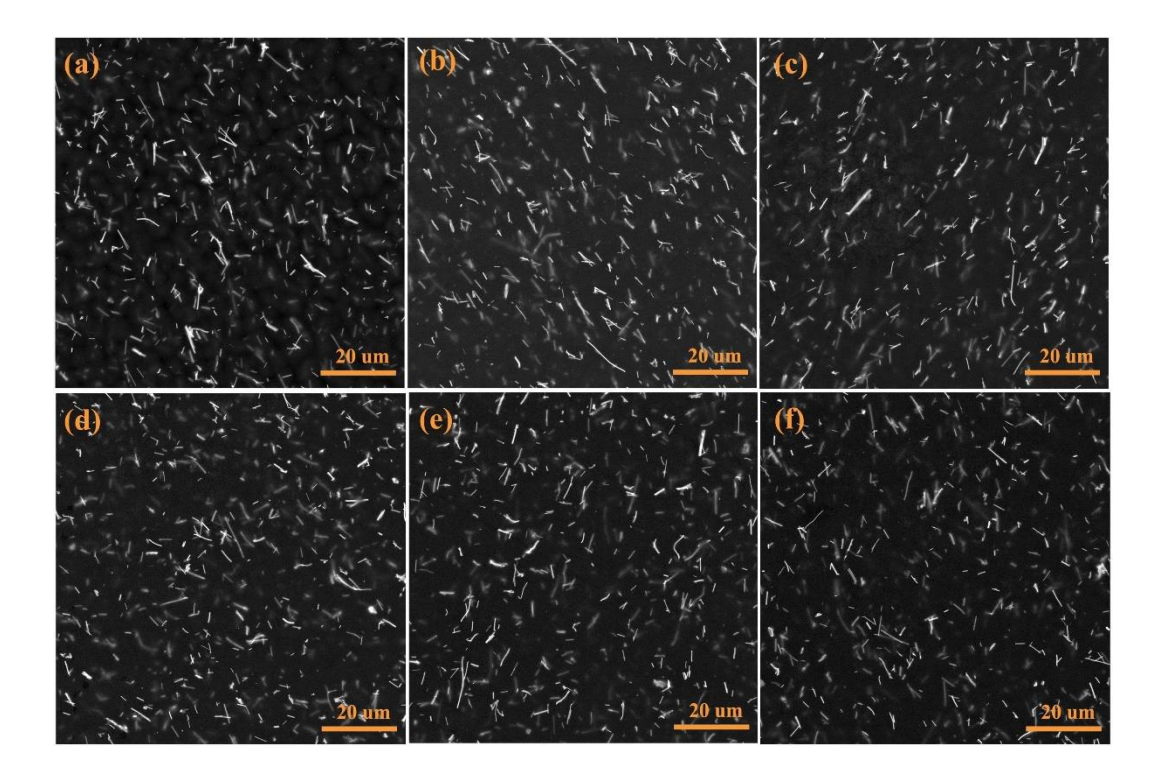


Figure 4. Surface SEM images of PVDF-TrFE composite films with different ceramic fillers. (a) Pure BCZT NWs. (b) 0.01Ag-BCZT NWs. (c) 0.02Ag-BCZT NWs. (d) 0.03Ag-BCZT NWs. (e) 0.04Ag-BCZT NWs. (f) 0.05Ag-BCZT NWs.

XRD analysis of the Ag-BCZT NWs/PVDF-TrFE composite films was carried out to investigate the crystalline structure of the materials. As shown in Figure 5a, the diffraction peak located at $2\theta = 19.7^{\circ}$ could be assigned to the reflections of the (110) and (200) orientation planes of PVDF-TrFE, thereby indicating the existence of the polar ferroelectric β -phase. ⁴⁵ Moreover, it can be observed that this diffraction peak was intensified after the decoration of Ag nanoparticles. The characteristic peak at 20 = 31.4° corresponds to the (110) plane of perovskite structured BCZT. The other diffraction peaks of BCZT cannot be easily observed due to low-level content of BCZT NWs. Moreover, the diffraction peaks of metallic Ag could not be detected in the composite films, since the loading content of Ag is also low. The FT-IR spectra of Ag-BCZT NWs/PVDF-TrFE composite films within the wavenumber between 700 and 1600 cm⁻¹ is presented in **Figure 5**b. It can be seen that all composite films possess almost the same phase composition. The characteristic peak at wavenumber 766cm⁻¹ is attributed to the nonpolar α -phase, whereas, the vibration bands at 843 cm⁻¹ and 1276 cm⁻¹ are assigned to the polar β-phase, according to previous reports.³³, ⁴⁶ In addition, the composite films are proved to possess high content of β -phase content, as shown in Figure S2. The results of FT-IR spectra reveal the phase composition of the PVDF-TrFE composite films, which is in accordance with the XRD results.

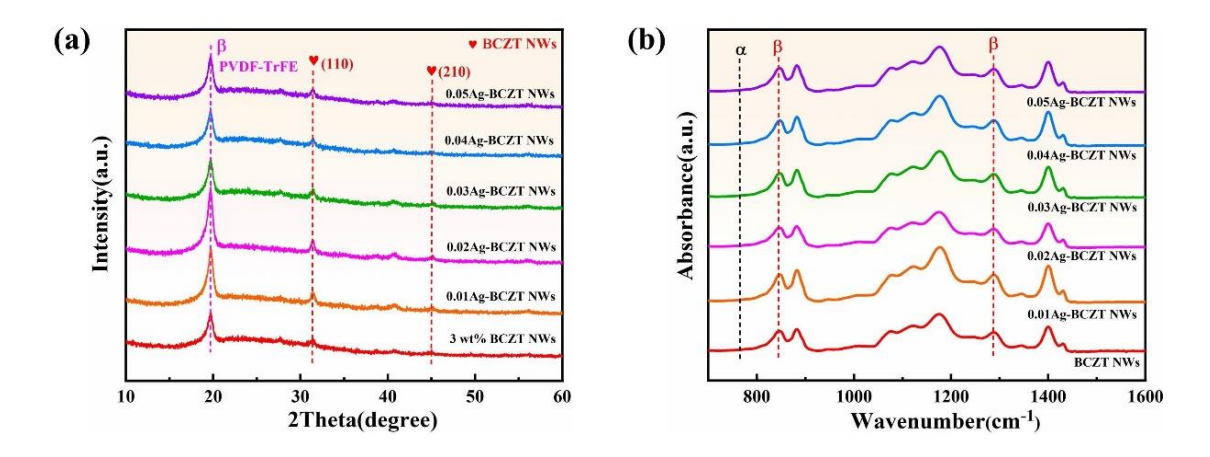


Figure 5. (a) XRD patterns of the Ag-BCZT NWs/PVDF-TrFE composite films. (b) FT-IR spectra of the Ag-BCZT NWs/PVDF-TrFE composite films.

The effect of Ag nanoparticles loading content on the dielectric properties of the PVDF-TrFE composite films is further investigated. The dielectric constant and dielectric loss as a function of frequency are presented in Figure 6a-b. As shown in Figure 6a, the dielectric constant of all the composite films decreased with an increase of frequency due to the confinement of dipoles and ionic migration at high frequency.⁴⁷ The dielectric loss initially increased with increasing frequency and then began to decrease, which can be attributed to the relaxation of PVDF-TrFE dipole polarization. 48 The dielectric constant and loss of xAg-BCZT NWs/PVDF-TrFE (x = 0, 0.01, 0.02, 0.03,0.04 and 0.05) composite films at 1 kHz is shown in **Figure 6**c. It can be seen that all the composite films exhibit a higher dielectric constant than that of pure PVDF-TrFE; this is due to the intrinsic high dielectric constant of BCZT. Moreover, the dielectric constant of xAg-BCZT NWs/PVDF-TrFE composite films is higher than that of the composite film without the decoration of Ag nanoparticles. When the Ag nanoparticles were deposited on the surface of BCZT NWs, many interfaces exist between the one-dimensional nanowires and Ag nanoparticles, which

is beneficial for the accumulation of space charges. As a result of this charge accumulation, the interfacial polarization is strengthened, leading to the enhancement of dielectric constant.⁴⁹ The dielectric constant of *x*Ag-BCZT NWs/PVDF-TrFE composite films increases with the increasing loading content of Ag nanoparticles. However, it begins to decrease when the loading content reaches 0.05M, which can be ascribed to the agglomeration of Ag nanoparticles, see **Figure 2**f. The dielectric loss of all the composite films at 1 kHz is maintained at a low level, which is beneficial to enhance the breakdown strength and reduce conductive losses when operating as a piezoelectric nanogenerator. Moreover, it can be observed from **Figure 6**d that the conductivities of the Ag-BCZT NWs/PVDF-TrFE composite films slightly increases with the loading content of Ag nanoparticles due to the conductive nature of metallic

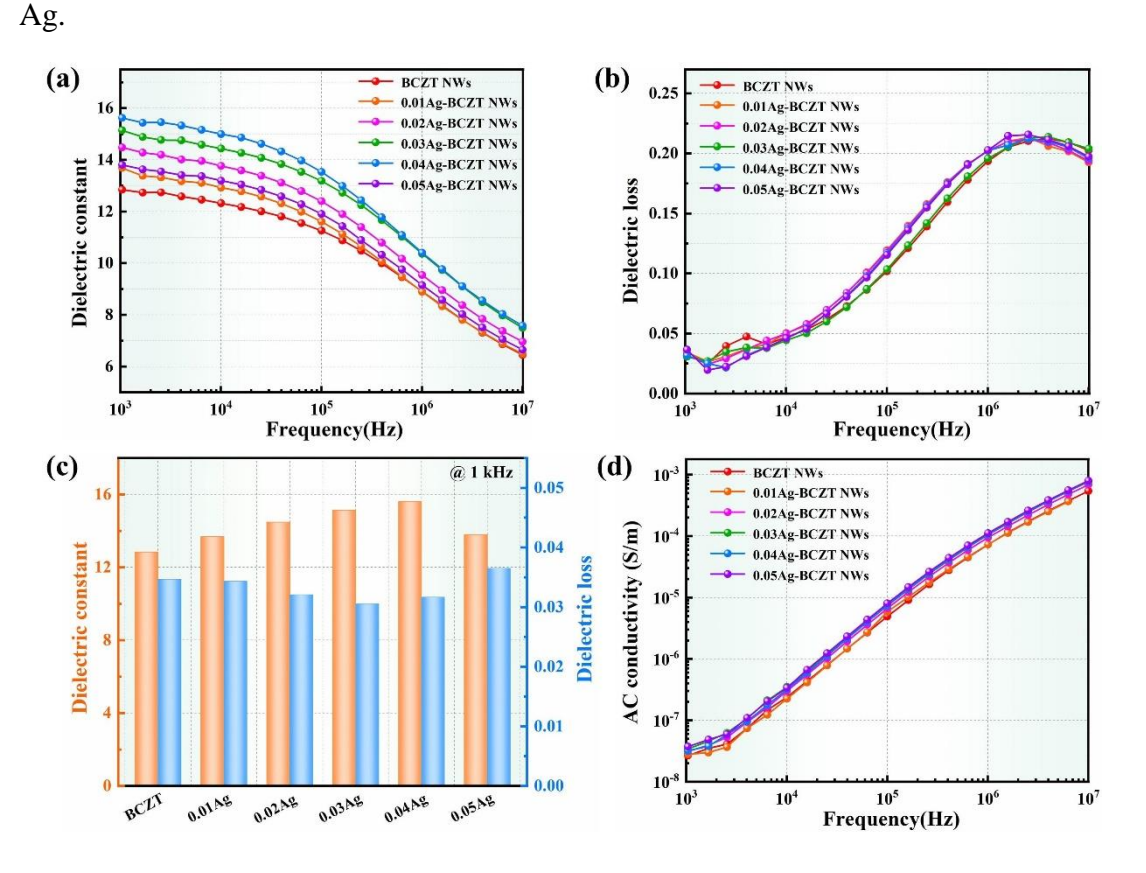


Figure 6. Dielectric properties of Ag-BCZT NWs/PVDF-TrFE composite films. (a)

Dielectric constant. (b) Dielectric loss. (c) Comparison of dielectric constant and loss at 1 kHz. (d) AC conductivity.

The ferroelectric properties of the Ag-BCZT NWs/PVDF-TrFE composite films are now estimated. Figure 7a shows the ferroelectric polarization-electric field hysteresis loops of the composite films at an electric field of 100 kV/mm. All the composite films exhibit a symmetrical ferroelectric hysteresis loop, indicating that the Ag-BCZT NWs/PVDF-TrFE composite films possess a good ferroelectric response. It can be seen from Figure 7b that the remnant polarization of the composite films increases first with an increase in Ag nanoparticle loading content, which then begins to decrease when the loading content is greater than 0.04. The decoration of Ag nanoparticles can enhance the local electric field in the BCZT NWs, where the polarization of the composite and the transfer of free charges becomes much easier.⁴⁹ Therefore, the remnant polarization of the composite films can be enhanced. However, the remnant polarization of 0.05Ag-BCZT NWs/PVDF-TrFE composite film significantly decreases, since the agglomeration of Ag nanoparticles can enhance the leakage current density. 50 Moreover, the coercive field decreased from 53.7 to 44.3 kV mm⁻¹ when the loading content of Ag nanoparticles increases from 0 to 0.04, then it increased slightly to 48.3 kV/mm for the 0.05Ag-BCZT NWs/PVDF-TrFE composite film. The reduction in coercive field due to the presence of electric field concentrations in the composite structure allows the Ag-BCZT NWs/PVDF-TrFE composite films to pole to a greater extent at a reduced externally applied electric field.

The electric breakdown strength is an important parameter for PVDF-TrFE based composites. A two-parameter statistical Weibull distribution was used to evaluate the breakdown strength, as shown in **Figure 7**c. This distribution can be described by the following equation:⁵¹

$$P(E) = 1 - \left[-\left(\frac{E}{E_h}\right)^{\beta} \right] \tag{1}$$

Where P(E) is the cumulative probability of electric failure, E is the measured electric breakdown strength, E_b represents the characteristic breakdown strength when P(E) is 0.632, β is the shape parameter. The electric breakdown strength E_b and shape parameter β of Ag-BCZT NWs/PVDF-TrFE composite films are summarized in **Figure 7d**. It can be observed that the electric breakdown strength of the composite films decreased from 214 kV/mm to 165 kV/mm with increasing Ag nanoparticles loading content. The shape parameter β represents the scatter of the measured electric breakdown strength. The lowest value of $\beta = 9.37$ was obtained in the sample of 0.05Ag-BCZT NWs/PVDF-TrFE composite film. The lower the value of β for the PVDF-TrFE composite film, the lower the quality and stability of the composite films and the greater the scatter in dielectric strength. Therefore, a high loading content of Ag nanoparticles can lead to a low electric breakdown strength and poor stability of the composite films.

As shown in **Figure 7**e, the piezoelectric d_{33} coefficient first increases with increasing Ag nanoparticle loading content and then begins to decrease. The piezoelectric voltage coefficient $(g_{33} = d_{33}/\varepsilon_{33}^T \varepsilon_0)$, which is a measure of the electric field per unit stress, exhibits the same trend, where a maximum value of $g_{33} \sim 203$ mV

m/N was obtained with the 0.04Ag-BCZT NWs/PVDF-TrFE composite film. The piezoelectric energy harvesting figures of merit can also be calculated by the following equation:

$$FoM_{33} = \frac{d_{33}^2}{\varepsilon_0 \varepsilon_{33}^T} \tag{2}$$

Where FoM_{33} is a piezoelectric energy harvesting figure of merit, d_{33} is the piezoelectric charge coefficient, ε_0 is the permittivity of free space, and ε_{33}^T is the relative permittivity at constant stress. It can be seen from **Figure 7**f that the FoM_{33} increased from 3.82×10^{-12} to 5.68×10^{-12} m²/N with increasing Ag nanoparticle loading content and then begins to decrease, where the highest value is achieved by the sample of 0.04Ag-BCZT NWs/PVDF-TrFE composite film; this value is 49% higher than that of pure BCZT NWs/PVDF-TrFE composite film. Therefore, 0.04Ag-BCZT/PVDF-TrFE composite film is more suitable for piezoelectric nanogenerator applications.

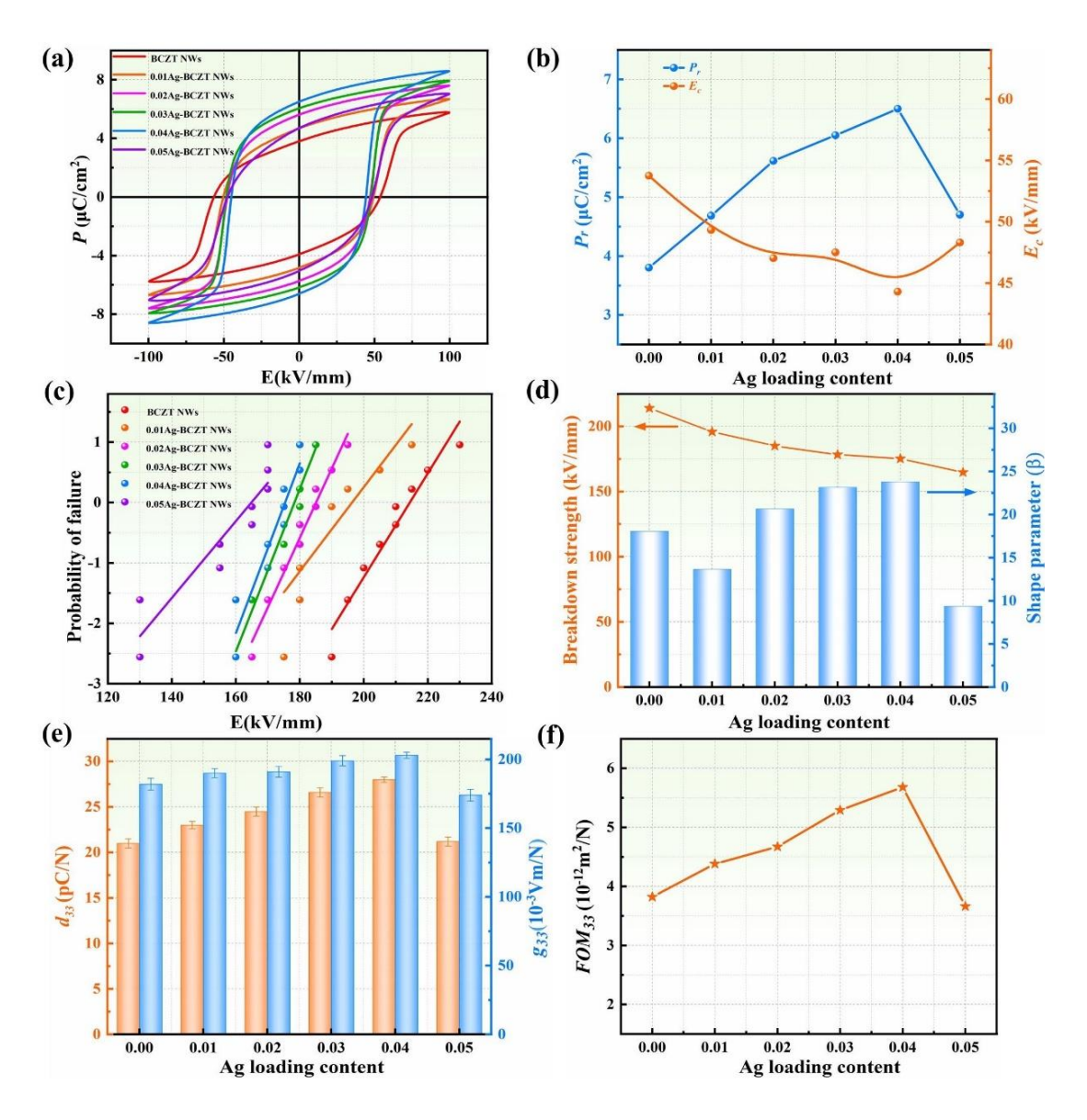


Figure 7. Ferroelectric and piezoelectric properties of Ag-BCZT NWs/PVDF-TrFE composite films. (a) Ferroelectric hysteresis loops. (b) Remnant polarization and coercive field. (c) Weibull distributions. (d) Breakdown strength and shape parameter. (e) Piezoelectric coefficient (d_{33}) and piezoelectric voltage coefficient (g_{33}) . (f) Piezoelectric energy harvesting figure of merit (FoM_{33}) .

Finite element analysis was performed by COMSOL 5.4 software to investigate the effect of Ag nanoparticles decoration on the electric field distribution and piezoelectric potential of PVDF-TrFE composite films. Two 2D models were created,

where the applied electric field and mechanical load were set to be 30 kV/mm and 10 N, respectively. Simulation results are presented in Figure 8. As shown in Figure 8a-b, the maximum electric field strength of the pure BCZT NWs/PVDF-TrFE composite film was 9.51×10^8 V/m, and after the introduction a conductor the maximum electric field strength reached 7.04×10^9 V/m after the decoration of Ag nanoparticles, which is 6.4 times higher than that of pure BCZT NWs/PVDF-TrFE composite film. This demonstrates that the decoration of Ag nanoparticles on BCZT NWs is beneficial to the polarization of the composite films due the existence of electric field concentrations.⁵² Moreover, the piezoelectric potential generated by Ag-BCZT NWs/PVDF-TrFE composite film is higher than that of pure BCZT NWs/PVDF-TrFE composite film under the same mechanical stress, see **Figure 8**c-d. The simulation results of electric field distribution and piezoelectric potential indicate that the decoration of Ag nanoparticles aids the polarization and output performance of BCZT NWs/PVDF-TrFE composite films. It should be noted that a careful balance is needed due to the presence of conductive inclusions in the ferroelectric composite, where the addition of Ag can lower the coercive field and increase the degree of poling due to the presence of electric field concentrations (Figure 8), while the existence of field concentrations can also reduce the breakdown strength (Figure 7d).

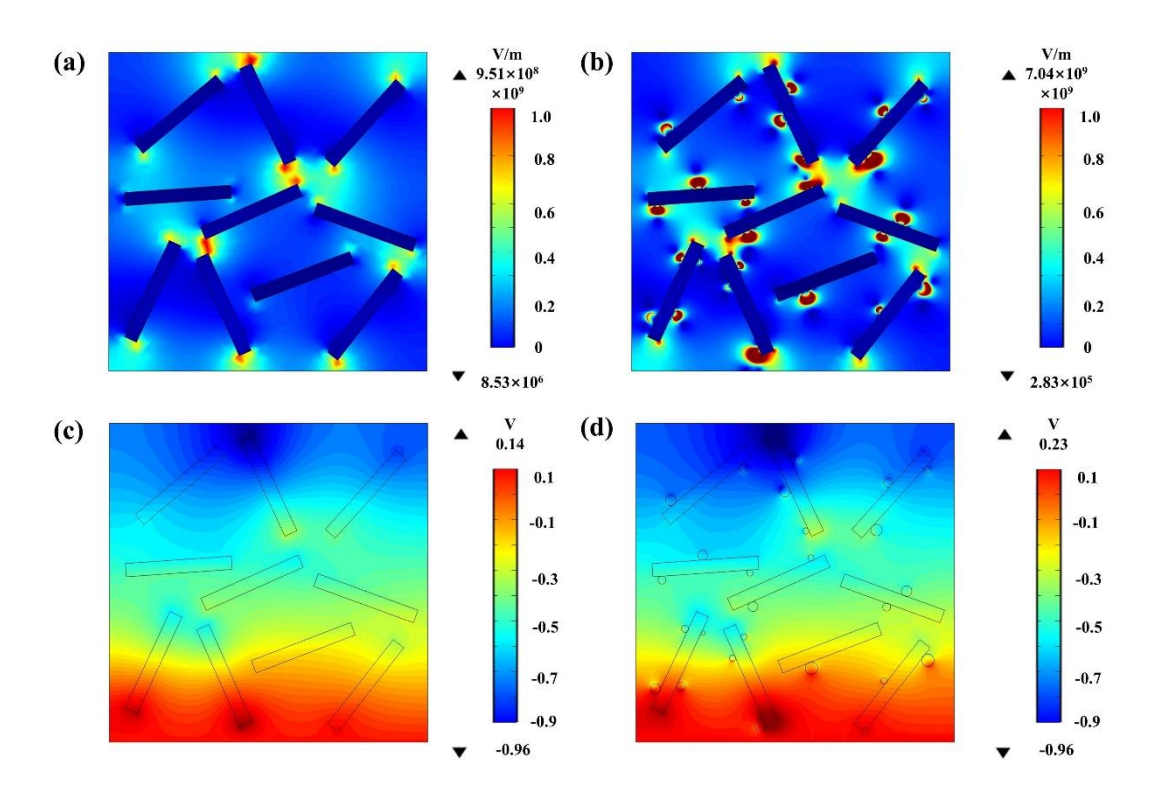


Figure 8. Electric field distribution of (a) BCZT NWs/PVDF-TrFE composite film. (b) Ag-BCZT NWs/PVDF-TrFE composite film. Piezoelectric potential of (c) BCZT NWs/PVDF-TrFE composite film. (d) Ag-BCZT NWs/PVDF-TrFE composite film.

The 0.04Ag-BCZT NWs/PVDF-TrFE composite film was selected for further characterization of piezoelectric energy harvesting performance due to it exhibiting the highest piezoelectric energy harvesting figure of merit. The output voltage of the composite film under different pressure at a frequency of 2 Hz is presented in **Figure 9a** and **Figure 9b**. It can be observed that the open circuit voltage increases almost linearly with increasing pressure, the maximum output voltage could reach 3.5 V under the pressure of 165 kPa, which is 2.3 times compared with that of pure BCZT NWs/PVDF-TrFE composite film without Ag nanoparticles decoration, as shown in **Figure S3**. Moreover, it can be observed from **Figure S4** that the short circuit current is approximately 1.8 μA under the same pressure. The enhanced output performance

can be attributed to the deposition of Ag nanoparticles on BCZT nanowires, where the working mechanism of the flexible piezoelectric energy harvester is shown in Figure S5. The ferroelectric dipoles are oriented along the direction of applied electric field and when a compressive force is applied on the piezoelectric energy harvester, the polarization is reduced as the dipole moment along the thickness direction is reduced. A potential difference is generated across the material, allowing electrons to flow through an external circuit. With the removal of external force, the polarization returns to its original state, and electrons flow in an opposite direction to maintain the electrical balance. During this process, the interface between Ag nanoparticles and BCZT nanowires can be regarded as a Schottky barrier, which is beneficial for the transfer of free charges during the deformation process. 16,53 A polarization switching test was conducted to confirm that the output voltage signal is originated from the piezoelectric effect, as shown in Figure 9c. The output voltage and current as a function of load resistance ranging from 500 k Ω to 100 M Ω are shown in **Figure 9**d. The output voltage of the flexible piezoelectric nanogenerator increases steadily with increasing load resistance, while the output current decreases, which can be attributed to the greater resistance to current flow with an increase in load resistance. The maximum output power of 4.5 mW/m² was achieved with a load resistance of 4 M Ω , see Figure 9e. Moreover, the durability and stability of the flexible piezoelectric energy harvester was evaluated by applying and releasing a vertical pressure of 165 kPa with the frequency of 2 Hz. It can be seen from Figure S6 that the output voltage of the flexible piezoelectric energy harvester remains almost stable after 3000 cycles, indicating the excellent mechanical stability and durability. As shown in **Figure9**f, an output voltage of 4 V was obtained under light finger tapping. Furthermore, the flexible piezoelectric nanogenerator can generator an output voltage of approximately 6.5 V under an impact at a large force by a fist, as shown in **Figure S5**, indicating that the flexible piezoelectric nanogenerator can harvest mechanical energy.

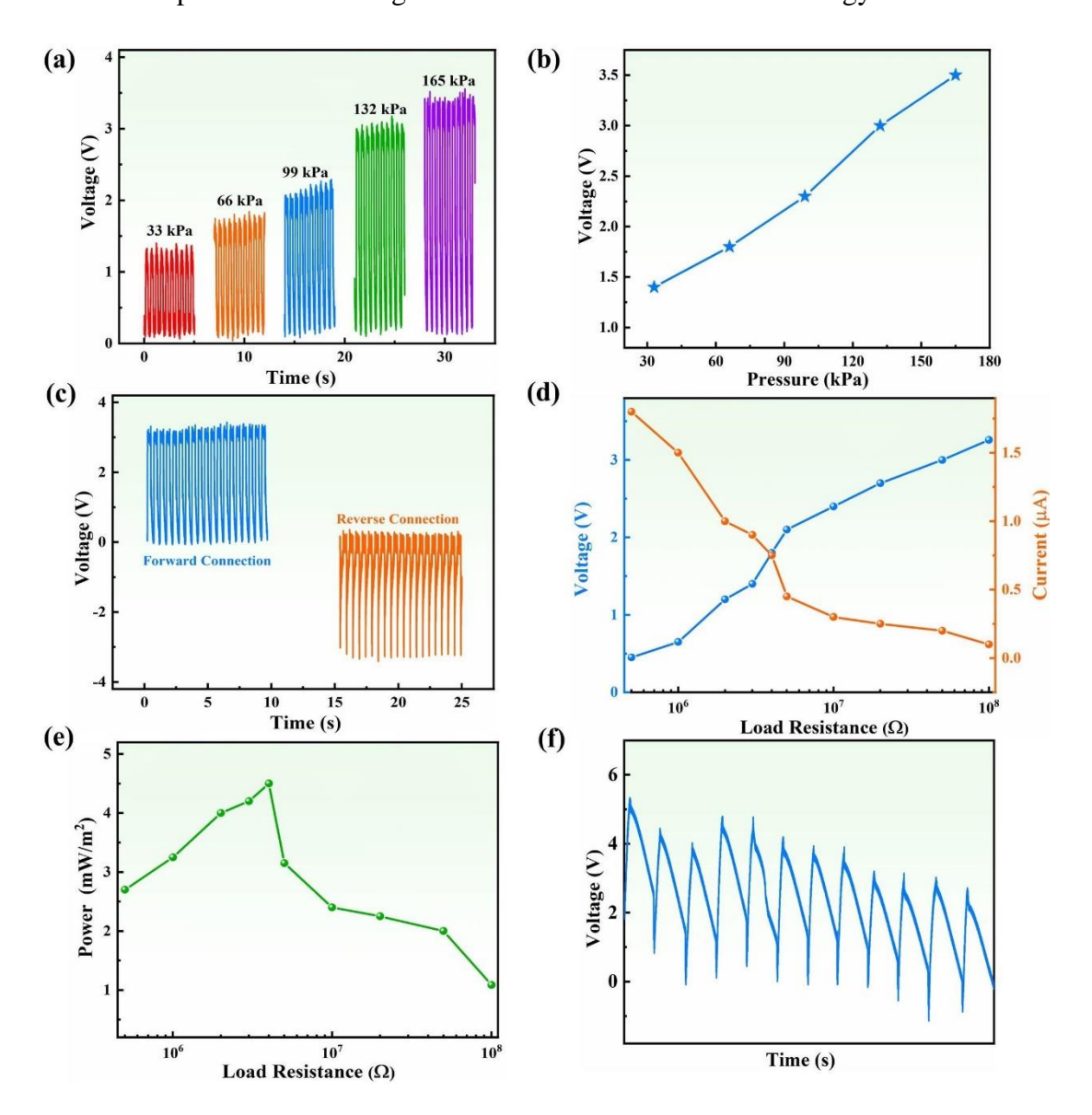


Figure 9. (a) Output voltage produced from the piezoelectric nanogenerator. (b) Output voltage as a function of pressure. (c) Forward and reverse connection of output voltage under the pressure of 165 kPa. (d) Voltage and current with various load

resistances. (e) Output power with various load resistances. (f) Output voltage under finger tapping force.

4. Conclusion

This work has developed a new approach to produce high performance piezoelectric composite films based on a low level of Ag-decorated ferroelectric BCZT heterostructures within a flexible ferroelectric PVDF-TrFE polymer matrix. The prepared composite film was used to fabricate flexible piezoelectric nanogenerator to harvest mechanical energy at a range of dynamic forces. Modelling and detailed characterization of the composite materials has shown that the decoration of BCZT nanowires with conductive Ag nanoparticles can increase the local electric field in the vicinity of the BCZT nanowires during the poling process, thereby leading to an enhancement in the degree of polarization and an increase the piezoelectric energy harvesting performance. With an increase in Ag nanoparticle loading content, the piezoelectric coefficient initially increases and then begins to decrease when the conductive silver particles begin to agglomerate and increase the level of conductive losses. The highest piezoelectric coefficient of $d_{33} \sim 28$ pC/N was obtained in the sample of 0.04Ag-BCZT NWs/PVDF-TrFE composite film, which also possess the piezoelectric energy harvesting figures of merit of 5.68×10⁻¹² m²/N, which is 49% higher than the composite with no silver additions. The piezoelectric energy harvesting performance of 0.04Ag-BCZT NWs/PVDF-TrFE composite film was also evaluated, where the output voltage generated by the sample could reach 3.5 V, which is 2.3 times compared with that of pure BCZT NWs/PVDF-TrFE composite film, with the maximum output power density of 4.5 mW/m². The flexible piezoelectric nanogenerator is demonstrated to have the ability to harvest mechanical energy for a range of dynamic loads (33 – 165 kPa) at an extended number of cycles. As a result, this work therefore provides a new approach for the fabrication of high performance flexible polymer-based piezoelectric nanogenerators by careful tailoring of the electric field distribution, coercive field, degree of polarization and dielectric strength.

ASSOCIATED CONTENT

Supporting Information

Cross-sectional SEM images and β phase content of the Ag-BCZT NWs/PVDF-TrFE composite films; output voltage of pure BCZT NWs/PVDF-TrFE composite film; output current of 0.04Ag-BCZT NWs/PVDF-TrFE composite film; working mechanism of the flexible piezoelectric energy harvester; cycling test data; output voltage under fist beating.

AUTHOR INFORMATION

Corresponding Authors

Yan Zhang - State Key Laboratory of Powder Metallurgy, Central South University, Changsha, Hunan 410083, China.

Xi Yuan - College of Chemistry and Chemical Engineering, Central South University, Changsha, Hunan 410083, China.

Authors

Mingyang Yan - State Key Laboratory of Powder Metallurgy, Central South University, Changsha, Hunan 410083, China

Shengwen Liu - State Key Laboratory of Powder Metallurgy, Central South University, Changsha, Hunan 410083, China.

Yuan Liu - State Key Laboratory of Powder Metallurgy, Central South University, Changsha, Hunan 410083, China

Zhida Xiao - State Key Laboratory of Powder Metallurgy, Central South University, Changsha, Hunan 410083, China

Di Zhai - State Key Laboratory of Powder Metallurgy, Central South University, Changsha, Hunan 410083, China

Kechao Zhou - State Key Laboratory of Powder Metallurgy, Central South University, Changsha, Hunan 410083, China

Qingping Wang - Department of Mechanical Engineering, University of Bath, United Kingdom, Bath, BA2 7AY, UK

Dou Zhang - State Key Laboratory of Powder Metallurgy, Central South University, Changsha, Hunan 410083, China

Chris Bowen - Department of Mechanical Engineering, University of Bath, United Kingdom, Bath, BA2 7AY, UK

Author Contributions

Mingyang Yan: Conceptualization, Experiment, Investigation, Writing - original draft. Shengwen Liu: Experiment, Investigation. Yuan Liu: preparation of BCZT

nanowires. Zhida Xiao: Investigation, Software. Xi Yuan: Conceptualization, Supervision. Di Zhai: Finite Element Analysis. Kechao Zhou: Conceptualization, Supervision. Qingping Wang: Conceptualization, Investigation. Dou Zhang: Writing - review & editing. Chris Bowen: Writing - review & editing. Yan Zhang: Supervision, Conceptualization, Writing - review & editing.

ACKNOWLEDGEMENTS

The authors acknowledge the National Key Research and Development Program (2022YFB3807400) and the National Natural Science Foundation of China (No.52172134, 52204263), Key Research and Development Project of Hunan Province (No. 2020WK2004), Overseas Talent Introduction Project of China, Hundred Youth Talents Program of Hunan and State Key Laboratory of Powder Metallurgy, Central South University, Changsha, China. Also, this work was supported by the Fundamental Research Funds for the Central Universities of Central South University.

Declaration of Competing Interest

The authors declare that they have no known competing financial interests or personal relationships that could have appeared to influence the work reported in this paper.

References

1. Shepelin, N. A.; Glushenkov, A. M.; Lussini, V. C.; Fox, P. J.; Dicinoski, G. W.; Shapter, J. G.; Ellis, A. V. New developments in composites, copolymer technologies

- and processing techniques for flexible fluoropolymer piezoelectric generators for efficient energy harvesting. *Energy Environ. Sci.* **2019**, *12*, 1143-1176.
- 2. Deng, W.; Zhou, Y.; Libanori, A.; Chen, G.; Yang, W.; Chen, J. Piezoelectric nanogenerators for personalized healthcare. *Chem. Soc. Rev.* **2022**, *51*, 3380-3435.
- 3. Wu, Y.; Qu, J.; Chu, P. K.; Shin, D.-M.; Luo, Y.; Feng, S.-P. Hybrid photovoltaic-triboelectric nanogenerators for simultaneously harvesting solar and mechanical energies. *Nano Energy* **2021**, *89*, 106376.
- 4. Hong, Y.; Wang, B.; Long, Z.; Zhang, Z.; Pan, Q.; Liu, S.; Luo, X.; Yang, Z. Hierarchically Interconnected Piezoceramic Textile with a Balanced Performance in Piezoelectricity, Flexibility, Toughness, and Air Permeability. *Adv. Funct. Mater.* **2021**, *31*, 2104737.
- 5. Khan, A. A.; Huang, G.; Rana, M. M.; Mei, N.; Biondi, M.; Rassel, S.; Tanguy, N.; Sun, B.; Leonenko, Z.; Yan, N.; Wang, C.; Xu, S.; Ban, D. Superior transverse piezoelectricity in organic-inorganic hybrid perovskite nanorods for mechanical energy harvesting. *Nano Energy* **2021**, *86*, 106039.
- 6. Liu, L.; Guo, X.; Lee, C. Promoting smart cities into the 5G era with multi-field Internet of Things (IoT) applications powered with advanced mechanical energy harvesters. *Nano Energy* **2021**, *88*, 106304.
- 7. Yan, M.; Xiao, Z.; Ye, J.; Yuan, X.; Li, Z.; Bowen, C.; Zhang, Y.; Zhang, D. Porous ferroelectric materials for energy technologies: current status and future perspectives. *Energy Environ. Sci.* **2021**, *14*, 6158-6190.
- 8. Rana, M. M.; Khan, A. A.; Huang, G.; Mei, N.; Saritas, R.; Wen, B.; Zhang, S.;

- Voss, P.; Abdel-Rahman, E.; Leonenko, Z.; Islam, S.; Ban, D. Porosity Modulated High-Performance Piezoelectric Nanogenerator Based on Organic/Inorganic Nanomaterials for Self-Powered Structural Health Monitoring. *ACS Appl Mater Interfaces* **2020**, *12*, 47503-47512.
- 9. Wu, T.; Song, Y.; Shi, Z.; Liu, D.; Chen, S.; Xiong, C.; Yang, Q. High-performance nanogenerators based on flexible cellulose nanofibril/MoS₂ nanosheet composite piezoelectric films for energy harvesting. *Nano Energy* **2021**, *80*, 105541.
- 10. Ippili, S.; Jella, V.; Eom, S.; Hong, S.; Yoon, S. G. Light-Driven Piezo- and Triboelectricity in Organic-Inorganic Metal Trihalide Perovskite toward Mechanical Energy Harvesting and Self-powered Sensor Application. *ACS Appl Mater Interfaces* **2020**, *12*, 50472-50483.
- 11. Jin, L.; Ma, S.; Deng, W.; Yan, C.; Yang, T.; Chu, X.; Tian, G.; Xiong, D.; Lu, J.; Yang, W. Polarization-free high-crystallization β-PVDF piezoelectric nanogenerator toward self-powered 3D acceleration sensor. *Nano Energy* **2018**, *50*, 632-638.
- 12. Zhai, W.; Nie, J.; Zhu, L. Enhanced Flexible Poly(vinylidene fluoride-trifluorethylene) Piezoelectric Nanogenerators by SnSe Nanosheet Doping and Solvent Treatment. *ACS Appl Mater Interfaces* **2021**, *13*, 32278-32285.
- 13. Ye, S.; Cheng, C.; Chen, X.; Chen, X.; Shao, J.; Zhang, J.; Hu, H.; Tian, H.; Li, X.; Ma, L.; Jia, W. High-performance piezoelectric nanogenerator based on microstructured P(VDF-TrFE)/BNNTs composite for energy harvesting and radiation protection in space. *Nano Energy* **2019**, *60*, 701-714.

- 14. Niu, X.; Jia, W.; Qian, S.; Zhu, J.; Zhang, J.; Hou, X.; Mu, J.; Geng, W.; Cho, J.; He, J.; Chou, X. High-Performance PZT-Based Stretchable Piezoelectric Nanogenerator. *ACS Sustainable Chemistry & Engineering* **2018**, *7*, 979-985.
- 15. Lv, P.; Qian, J.; Yang, C.; Liu, T.; Wang, Y.; Wang, D.; Huang, S.; Cheng, X.; Cheng, Z. Flexible all-inorganic Sm-doped PMN-PT film with ultrahigh piezoelectric coefficient for mechanical energy harvesting, motion sensing, and human-machine interaction. *Nano Energy* **2022**, *97*, 107182.
- 16. Wang, Z.; Zhang, Y.; Yang, S.; Hu, Y.; Wang, S.; Gu, H.; Wang, Y.; Chan, H. L.; Wang, J. (K,Na)NbO₃ nanofiber-based self-powered sensors for accurate detection of dynamic strain. *ACS Appl Mater Interfaces* **2015**, *7*, 4921-7.
- 17. Jin, C. C.; Liu, X. C.; Liu, C. H.; Wang, Y.; Hwang, H. L.; Wang, Q. High-performance BCTZ nanowires-based energy harvesting device and self-powered bio-compatible flexion sensor. *Mater. Des.* **2018**, *144*, 55-63.
- 18. Wu, Q.; Guo, H.; Sun, H.; Liu, X.; Sui, H.; Wang, F. Flexible piezoelectric energy harvesters with graphene oxide nanosheets and PZT-incorporated P(VDF-TrFE) matrix for mechanical energy harvesting. *Ceram. Int.* **2021**, *47*, 19614-19621.
- 19. Cho, Y.; Jeong, J.; Choi, M.; Baek, G.; Park, S.; Choi, H.; Ahn, S.; Cha, S.; Kim, T.; Kang, D.-S.; Bae, J.; Park, J.-J. BaTiO₃@PVDF-TrFE nanocomposites with efficient orientation prepared via phase separation nano-coating method for piezoelectric performance improvement and application to 3D-PENG. *Chem. Eng. J.* **2022**, *427*, 131030.
- 20. Zhang, G.; Zhao, P.; Zhang, X.; Han, K.; Zhao, T.; Zhang, Y.; Jeong, C. K.; Jiang,

- S.; Zhang, S.; Wang, Q. Flexible three-dimensional interconnected piezoelectric ceramic foam based composites for highly efficient concurrent mechanical and thermal energy harvesting. *Energy Environ. Sci.* **2018**, *11*, 2046-2056.
- 21. Zhou, X.; Parida, K.; Halevi, O.; Liu, Y.; Xiong, J.; Magdassi, S.; Lee, P. S. All 3D-printed stretchable piezoelectric nanogenerator with non-protruding kirigami structure. *Nano Energy* **2020**, *72*, 104676.
- 22. Park, K. I.; Bae, S. B.; Yang, S. H.; Lee, H. I.; Lee, K.; Lee, S. J. Lead-free BaTiO₃ nanowires-based flexible nanocomposite generator. *Nanoscale* **2014**, *6*, 8962-8.
- 23. Wang, Q.; Yang, D.; Qiu, Y.; Zhang, X.; Song, W.; Hu, L. Two-dimensional ZnO nanosheets grown on flexible ITO-PET substrate for self-powered energy-harvesting nanodevices. *Appl. Phys. Lett.* **2018**, *112*, 063906.
- 24. Zhang, D.; Yang, Z.; Li, P.; Pang, M.; Xue, Q. Flexible self-powered high-performance ammonia sensor based on Au-decorated MoSe₂ nanoflowers driven by single layer MoS₂-flake piezoelectric nanogenerator. *Nano Energy* **2019**, *65*, 611-619.
- 25. Yi, Z.; Wang, Z.; Nian, W.; Wang, T.; Chen, H.; Cheng, Z. High Energy Storage Density of Sandwich-Structured Na_{0.5}Bi_{0.5}TiO₃/PVDF Nanocomposites Enhanced by Optimizing the Dimensions of Fillers. *ACS Applied Energy Materials* **2021**, *4*, 13528-13537.
- 26. Tang, H.; Zhou, Z.; Sodano, H. A. Relationship between BaTiO₃ nanowire aspect ratio and the dielectric permittivity of nanocomposites. *ACS Appl Mater Interfaces*

- 27. Yan, J.; Liu, M.; Jeong, Y. G.; Kang, W.; Li, L.; Zhao, Y.; Deng, N.; Cheng, B.; Yang, G. Performance enhancements in poly(vinylidene fluoride)-based piezoelectric nanogenerators for efficient energy harvesting. *Nano Energy* **2019**, *56*, 662-692.
- 28. Hu, D.; Yao, M.; Fan, Y.; Ma, C.; Fan, M.; Liu, M. Strategies to achieve high performance piezoelectric nanogenerators. *Nano Energy* **2019**, *55*, 288-304.
- 29. Zhang, H.; Marwat, M. A.; Xie, B.; Ashtar, M.; Liu, K.; Zhu, Y.; Zhang, L.; Fan, P.; Samart, C.; Ye, Z. G. Polymer Matrix Nanocomposites with 1D Ceramic Nanofillers for Energy Storage Capacitor Applications. *ACS Appl Mater Interfaces* **2020**, *12*, 1-37.
- 30. Fu, J.; Hou, Y.; Gao, X.; Zheng, M.; Zhu, M. Highly durable piezoelectric energy harvester based on a PVDF flexible nanocomposite filled with oriented BaTi₂O₅ nanorods with high power density. *Nano Energy* **2018**, *52*, 391-401.
- 31. Lu, C.; Zhang, L.; Xu, C.; Yin, Z.; Zhou, S.; Wang, J.; Huang, R.; Zhou, X.; Zhang, C.; Yang, W.; Lu, J. Self-powered graphene quantum dot/poly(vinylidene fluoride) composites with remarkably enhanced mechanical-to-electrical conversion. *RSC Adv.* **2016**, *6*, 67400-67408.
- 32. Ke, K.; Pötschke, P.; Jehnichen, D.; Fischer, D.; Voit, B. Achieving β-phase poly(vinylidene fluoride) from melt cooling: Effect of surface functionalized carbon nanotubes. *Polymer* **2014**, *55*, 611-619.
- 33. Shi, K.; Chai, B.; Zou, H.; Shen, P.; Sun, B.; Jiang, P.; Shi, Z.; Huang, X. Interface induced performance enhancement in flexible BaTiO₃/PVDF-TrFE based

piezoelectric nanogenerators. Nano Energy 2021, 80, 105515.

- 34. Zhou, Z.; Du, X.; Luo, J.; Yao, L.; Zhang, Z.; Yang, H.; Zhang, Q. Coupling of interface effects and porous microstructures in translucent piezoelectric composites for enhanced energy harvesting and sensing. *Nano Energy* **2021**, *84*, 105895.
- 35. Huan, Y.; Zhang, X.; Song, J.; Zhao, Y.; Wei, T.; Zhang, G.; Wang, X. High-performance piezoelectric composite nanogenerator based on Ag/(K,Na)NbO₃ heterostructure. *Nano Energy* **2018**, *50*, 62-69.
- 36. Zhou, Z.; Zhang, Z.; Zhang, Q.; Yang, H.; Zhu, Y.; Wang, Y.; Chen, L. Controllable Core-Shell BaTiO₃@Carbon Nanoparticle-Enabled P(VDF-TrFE) Composites: A Cost-Effective Approach to High-Performance Piezoelectric Nanogenerators. *ACS Appl Mater Interfaces* **2020**, *12*, 1567-1576.
- 37. Shuai, C.; Liu, G.; Yang, Y.; Qi, F.; Peng, S.; Yang, W.; He, C.; Wang, G.; Qian, G. A strawberry-like Ag-decorated barium titanate enhances piezoelectric and antibacterial activities of polymer scaffold. *Nano Energy* **2020**, *74*, 104825.
- 38. Guan, X.; Xu, B.; Gong, J. Hierarchically architected polydopamine modified BaTiO₃@P(VDF-TrFE) nanocomposite fiber mats for flexible piezoelectric nanogenerators and self-powered sensors. *Nano Energy* **2020**, *70*, 104516.
- 39. Liu, Y.; Chang, Y.; Li, F.; Yang, B.; Sun, Y.; Wu, J.; Zhang, S.; Wang, R.; Cao, W. Exceptionally High Piezoelectric Coefficient and Low Strain Hysteresis in Grain-Oriented (Ba, Ca)(Ti, Zr)O₃ through Integrating Crystallographic Texture and Domain Engineering. *ACS Appl Mater Interfaces* **2017**, *9*, 29863-29871.
- 40. Cui, Y.; Zhang, T.; Feng, Y.; Zhang, C.; Chi, Q.; Zhang, Y.; Chen, Q.; Wang, X.;

- Lei, Q. Excellent energy storage density and efficiency in blend polymer-based composites by design of core-shell structured inorganic fibers and sandwich structured films. *Composites Part B: Engineering* **2019**, *177*, 107429.
- 41. Shafee, E. E.; Behery, S. M. Preparation, characterization and properties of novel 0–3 ferroelectric composites of Ba_{0.95}Ca_{0.05}Ti_{0.8}Zr_{0.2}O₃–poly(vinylidene fluoride-trifluoroethylene). *Mater. Chem. Phys.* **2012**, *132*, 740-746.
- 42. Yuan, M.; Cheng, L.; Xu, Q.; Wu, W.; Bai, S.; Gu, L.; Wang, Z.; Lu, J.; Li, H.; Qin, Y.; Jing, T.; Wang, Z. L. Biocompatible nanogenerators through high piezoelectric coefficient 0.5Ba(Zr_{0.2}Ti_{0.8})O₃-0.5(Ba_{0.7}Ca_{0.3})TiO₃ nanowires for in-vivo applications. *Adv Mater* **2014**, *26*, 7432-7.
- 43. Xu, X.; Chen, S.; Wu, Z.; Jia, Y.; Xiao, L.; Liu, Y. Strong pyro-electro-chemical coupling of Ba_{0.7}Sr_{0.3}TiO₃@Ag pyroelectric nanoparticles for room-temperature pyrocatalysis. *Nano Energy* **2018**, *50*, 581-588.
- 44. Xu, J.; Qin, T.; Chen, W.; Lv, J.; Zeng, X.; Sun, J.; Li, Y.-y.; Zhou, J. Synergizing piezoelectric and plasmonic modulation of Ag/BiFeO₃ fibrous heterostructure toward boosted photoelectrochemical energy conversion. *Nano Energy* **2021**, *89*, 106317.
- 45. Zhang, Y.; Zhou, L.; Gao, X.; Liu, C.; Chen, H.; Zheng, H.; Gui, J.; Sun, C.; Yu, L.; Guo, S. Performance-enhanced flexible piezoelectric nanogenerator via layer-by-layer assembly for self-powered vagal neuromodulation. *Nano Energy* **2021**, 89, 106319.
- 46. Rana, S. M. S.; Rahman, M. T.; Salauddin, M.; Sharma, S.; Maharjan, P.; Bhatta, T.; Cho, H.; Park, C.; Park, J. Y. Electrospun PVDF-TrFE/MXene Nanofiber

- Mat-Based Triboelectric Nanogenerator for Smart Home Appliances. *ACS Appl Mater Interfaces* **2021**, *13*, 4955-4967.
- 47. Zhang, Y.; Zhang, C.; Feng, Y.; Zhang, T.; Chen, Q.; Chi, Q.; Liu, L.; Wang, X.; Lei, Q. Energy storage enhancement of P(VDF-TrFE-CFE)-based composites with double-shell structured BZCT nanofibers of parallel and orthogonal configurations. *Nano Energy* **2019**, *66*, 104195.
- 48. Kim, J.; Ji, J.-H.; Shin, D.-J.; Yoon, S.; Ko, Y.-H.; Cho, K.-H.; Koh, J.-H. 2-Dimensional rGO introduced PMN-PT and P(VDF-TrFE) flexible films for enhanced piezoelectric energy harvester. *Appl. Surf. Sci.* **2019**, *494*, 1000-1006.
- 49. Sasmal, A.; Patra, A.; Devi, P. S.; Sen, S. Space charge induced augmented dielectric permittivity and improved energy harvesting ability of nano-Ag decorated ZnSnO₃ filled PVDF based flexible nanogenerator. *Composites Science and Technology* **2021**, *213*, 108916.
- 50. Luo, S.; Yu, S.; Sun, R.; Wong, C. P. Nano Ag-deposited BaTiO₃ hybrid particles as fillers for polymeric dielectric composites: toward high dielectric constant and suppressed loss. *ACS Appl Mater Interfaces* **2014**, *6*, 176-82.
- 51. Xiong, X.; Zhang, Q.; Yang, H. Ultra-Fine Gold Nanoparticles Enabled Au-BST NF/PVTC Composites to Have Excellent Energy Storage Performance. *ACS Applied Energy Materials* **2021**, *4*, 6511-6519.
- 52. Zeng, S.; Zhang, M.; Jiang, L.; Wang, Z.; Gu, H.; Xiong, J.; Du, Y.; Ren, L. Wearable Piezoelectric Nanogenerators Based on Core-Shell Ga-PZT@GaO_x Nanorod-Enabled P(VDF-TrFE) Composites. *ACS Appl Mater Interfaces* **2022**, *14*,

7990-8000.

53. Huan, Y.; Wei, T.; Wang, Z.; Shen, H.; Lin, X.; Huang, S.; Wang, X. Ultrahigh energy harvesting properties in Ag decorated potassium-sodium niobite particle-polymer composite. *Journal of Materiomics* **2020**, *6*, 355-363.

For Table of Contents Only

